6ICEGE 6th International Conference on Earthquake Geotechnical Engineering
1-4 November 2015
Christchurch. New Zealand

Liquefaction model calibration: element-level versus 1-D site response

J.R. Gingery[1], A. Elgamal[2], J.D. Bray[3]

ABSTRACT

Calibration of constitutive models for liquefaction is frequently carried out at the element level and then applied in the analysis of larger soil systems. Key mechanisms are at play in the soil system – like porewater pressure redistribution, non-uniform loading, wave reflection and inertial effects – that are not present in the simple single-element calibration case. This paper addresses the question of whether element-level calibrations are adequate when a broader and more complex soil-system response is considered. An effective stress constitutive model incorporating contraction, dilation and cyclic mobility is rigorously calibrated at the element level to a semi-empirical liquefaction triggering relationship. The calibrated model is then used in one-dimensional effective stress site response analyses for a variety of soil profiles and input ground motions. Excess porewater pressure ratio (r_u) results from the site response analyses are compared with factors of safety calculated for the site response profiles using the same semi-empirical triggering relationship that was used for the element-level calibration. The results show good agreement between the site response r_u values and the calculated factors of safety, indicating that for the cases studied, the element-level calibrations are valid for liquefaction triggering analysis of prototype soil systems.

Introduction and Background

There have been noteworthy increases in the sophistication and availability of numerical modeling tools for evaluating soil liquefaction problems. Numerous models are now available that can capture salient aspects of soil liquefaction such as contraction, dilation, and cyclic mobility. For models to produce reasonable and realistic results, they must be properly calibrated within the range of conditions (e.g., confining stresses and relative density) they will be employed.

It is common to carry out calibration work at the element level where boundary conditions and loading can be tightly controlled. Calibration for soil liquefaction triggering typically involves subjecting an element in direct simple shear (DSS) to cycles of uniform cyclic stress and adjusting parameters until the number of cycles to liquefaction is consistent with a target from some triggering criterion. Parameters determined through this calibration process are then used in prototype-scale models that are significantly more complex in terms of geometry, material heterogeneity, drainage, dynamic response, and loading. In particular, dynamic excitation of prototype-scale models in liquefaction analyses typically consists of an earthquake time history, which is a much more complex and irregular loading compared to the uniform cyclic stresses applied in the calibration.

[1]Kleinfelder, Inc., San Diego, California, jgingery@kleinfelder.com
[2]Dept. of Structural Engineering, University of California, San Diego, aelgamal@ucsd.edu
[3]Dept. of Civil and Environmental Engineering, University of California, Berkeley, jonbray@berkeley.edu

This paper presents a study where element-level calibration of a liquefaction constitutive model was performed, and then the calibrated model was used in prototype-scale one-dimensional (1D) site response analysis simulations. The model was calibrated to fit closely the predictions of a semi-empirical liquefaction triggering method. The site response analysis simulations were then performed for a range of soil relative densities, stratigraphic geometries, and input ground motions. The site response results were compared to the semi-empirical method's estimates of soil liquefaction triggering for the prototype profiles and ground motions.

The purpose of this work was to evaluate whether, for the cases considered, liquefaction model calibration conducted at the element level also holds true for the more complex prototype simulations. This work was originally performed as part of a broader study on the effects of liquefaction on ground motions (Gingery 2014).

Numerical Model

All of the simulations in this paper were performed using OpenSees (Open System for Earthquake Engineering Simulation), which is an open-source software platform for finite element and other engineering analyses (Mazzoni et al. 2010). The PressureDependentMultiYield02 (PDMY2) model was used with four-node quadrilateral u-p (fluid-solid) finite elements (Elgamal et al. 2002, 2003; Yang et al. 2003; Yang et al. 2008). The PDMY2 model uses a non-associative flow rule that allows for volumetrically contractive or dilative response as a result of shear loading. When employed with fluid-solid finite elements, the contractive/dilative response causes porewater pressure changes (excluding fully drained response scenarios). The model employs a strain-space mechanism that controls the cyclic accumulation of shear strain under liquefaction cyclic mobility conditions. These features permit modeling of salient characteristics of undrained or partially-drained cyclic response of liquefiable soils, such as shear-induced contraction and dilation, excess porewater pressure development, cyclic mobility and porewater flow.

Element-Level Calibration

The element level calibration is described in detail in Gingery (2014) and a brief overview is provided below. The model parameters required for calibration include small strain shear and bulk moduli, internal angle of friction, a shear stress versus shear strain relationship that provides the backbone in drained response, and an assortment of contraction and dilation parameters. The shear stress-strain relationship can either be specified automatically by the model based on the hyperbolic model of Hardin and Drnevich (1972) and the assigned strength parameters, or the user can specify a shear modulus reduction curve. In this work, the shear modulus reduction curves of Darendeli (2000) were used with a modification in the failure strain range to assure compatibility with the intended shear strength (Gingery and Elgamal 2013). The small strain shear modulus was calculated based on typical soil densities and the empirical shear wave velocity relationship of Brandenberg et al. (2010).

The contraction and dilation parameters were established by performing single element, undrained cyclic DSS simulations. The simulations were performed iteratively and the parameters adjusted to fit the results to the semi-empirical liquefaction triggering relationship of

Idriss and Boulanger (2008) for relative densities (D_r) from 30% to 90% and confining stresses ranging up to 8 atm. Parameters controlling post-liquefaction accumulation of strain during cyclic mobility were calibrated against cyclic simple shear data from Wu (2002). Table 1 summarizes the calibrated parameter set for various relative densities.

Table 1. Calibrated model parameters.

Parameter	**Relative Density, *Dr***				
	30%	**50%**	**70%**	**80%**	**90%**
User-defined G/G_{max} versus γ	Darendeli (2000) with PI = 0, OCR = 1 and $\sigma'_0 = \sigma'_{v0}$, adjusted for strength per Gingery and Elgamal (2013)				
Density, ρ [Mg/m^3]	1.70	1.83	1.97	2.03	2.10
Shear wave velocity, V_s [m/s]	$\ln(V_s) = 4.045 + 0.096\ln(N_{60}) + 0.236\ln(\sigma'_{v0})$ (Brandenberg et al. 2010)				
Ref. shear modulus, G_r [kPa]	$G_r = V_S^2 / \rho$				
Ref. bulk modulus, B_r [kPa]	$B_r = \frac{2G_r(1+\nu)}{3(1-2\nu)}$ (note a)				
DSS friction angle, φ_{DSS} [deg]	28	33	39	41	44
Model friction angle, φ [deg]	23.5	28.6	34.2	37.4	40.8
Cohesion, c [kPa]	0.1				
Shear strain at failure, γ_f [-]	Irrelevant for user-defined G/G_{max} vs. γ				
Ref. pressure, p'_r [kPa]	Set to σ'_{v0}				
Pressure dependent coef., d [-]	0.5				
Phase trans. angle, φ_{PT} [deg.]	20				
Contraction parameter 1, c_1 [-]	0.135	0.080	0.046	0.035	0.32
Contraction parameter 2, c_2 [-]	1.00	2.20	4.00	5.20	6.40
Contraction parameter 3, c_3 [-]	0.120	0.180	0.198	0.200	0.175
Dilation parameter 1, d_1 [-]	0.440	0.160	0.060	0.045	0.040
Dilation parameter 2, d_2 [-]	3.00	3.00	2.00	1.50	1.00
Dilation parameter 3, d_3 [-]	0.00	0.00	0.00	-0.17	-0.34
PT strain parameter, y_1 [-]	1.00	1.00	0.28	0.10	0.00

Note: (a) For the initial consolidation phase, ν is set to 0.499 so that a $K_0 = 1$ condition is achieved. For the dynamic loading phase, ν is set to 0.

Site Response Analyses

The calibrated model was used in a series of 1D site response analyses. A range of soil profiles and input ground motions were used as described below.

Soil Profiles

The analyses were performed for all combinations of three depths to the top of the liquefiable layer (z_{liq} = {1, 3, 10} m), three liquefiable layer thicknesses (T_{liq} = {1, 3, 10} m) and four liquefiable layer relative densities (D_r = {30, 50, 70, 80} %), for a total of $3 \times 3 \times 4 = 36$ soil profiles. The groundwater level was assumed at 1 m depth below the surface in all cases. Figure 1 presents a diagram of the soil profiles considered in the parametric analyses. The compliant base (Lysmer and Kuhlemeyer 1969) at the bottom of the profile was modeled as bedrock with a density of 2.16 Mg/m^3 and V_s of 560 m/s, and firm soil with a density of 2.16 Mg/m^3 and V_s of

335 m/s. The hydraulic conductivity of all of the soils was set to $1e10^{-3}$ cm/s, a value typical of silty sand to sand (Power 1992). Additional work is warranted to explore the important role of varying the hydraulic conductivity of soil layers within the profile.

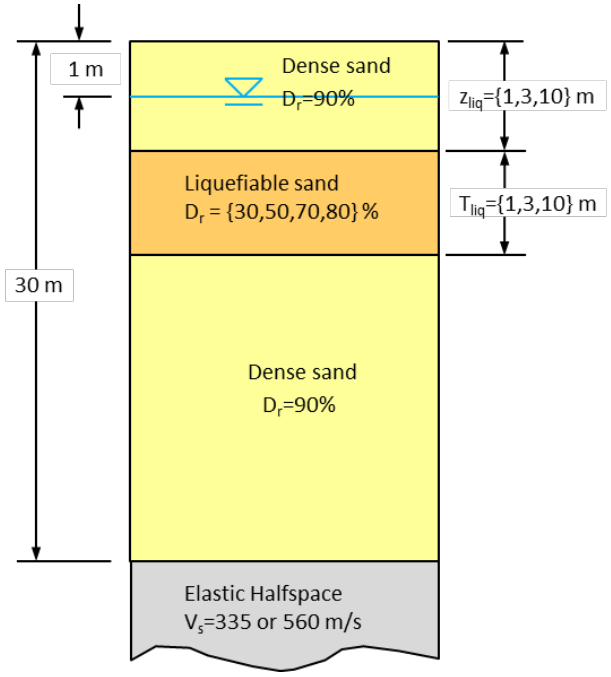

Figure 1. Soil profiles used in the conducted site response analyses.

Input Ground Motions

A suite of ground motions was selected to span ranges of magnitude and distance, faulting mechanism, and spectral shape and amplitude. The distance and magnitude pairings were limited to those that have been shown by Ambrayses (1988) to produce liquefaction. A total of 83 ground motions grouped into 8 magnitude-distance-V_{s30} bins were used (Table 2). Two of the bins are populated with pulse-like ground motions according to the definition of Baker (2007). As shown in Figure 2, the ground motions cover a wide range of amplitude and spectral shape. The minimum and maximum peak ground accelerations are 0.02 g and 0.9 g, respectively. All of the bins are from recording stations with $V_{s30} \geq$ 400 m/s (e.g., "soft rock" conditions where model bedrock V_s = 560 m/s) except for Bin 8 which represents firm soil conditions with 180 $\leq V_{s30} \leq$ 360 m/s (model half-space has V_s = 335 m/s).

The shallow crustal earthquake recordings in Bins 1-6 and 8 were obtained from the PEER NGA West 2 ground motion database (Seyhan et al. 2014). Bin 7 consists of 8 interplate subduction zone earthquake recordings that were obtained from the database compiled by Carlton (2014).

Table 2. Summary of magnitude and distance bins and the number of ground motions in each bin (in brackets).

Distance / **Magnitude** (V_{s30})	**Near Fault** R_{jb} **< 20 km**		**More Distant** R_{jb} **> 20 km**
	Non-Pulse	**Pulse**	
M_w ~9 Shallow Crustal ($V_{s30} \geq$ 400 m/s)	Not used		Bin 7 [8]
M_w = 7-8 Shallow Crustal ($V_{s30} \geq$ 400 m/s)	Bin 4 [8]	Bin 5 [8]	Bin 6 [22]
M_w = 6.5-7.5 Shallow Crustal (180 $\leq V_{s30} \leq$ 360 m/s)	Bin 8, R_{jb}=10-70 km, non-pulse [9]		
M_w = 6-7 Shallow Crustal ($V_{s30} \geq$ 400 m/s)	Bin 1 [8]	Bin 2 [13]	Bin 3 [7]

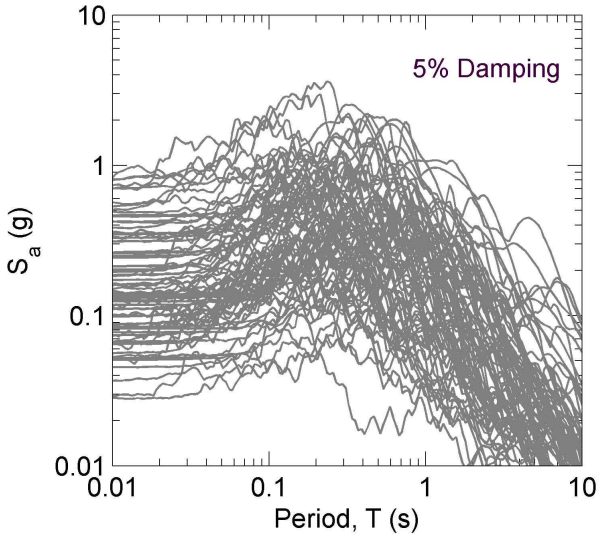

Figure 2. Acceleration response spectra (5% damped) for all the ground motions used in the seismic site response analyses.

Fidelity of the Model in Predicting Liquefaction Triggering

Factors of safety against liquefaction triggering were calculated for points at the top, middle and bottom of the potentially liquefiable layer using the Idriss and Boulanger (2008) method. These factors of safety (FS_{IB08}) were calculated using input ground motion magnitude and the surface PGA from a site response analysis that was conducted without porewater pressure generation (for consistency with the assumptions of Idriss and Boulanger 2008). The stress reduction factors were based on the magnitude-dependent relationship of Idriss and Boulanger (2008).

Figure 3 presents three examples of effective stress and excess porewater pressure ratio profiles and calculated FS_{IB08}. The r_u values were calculated based on the initial effective stress (σ'_{v0}) and the minimum effective stress that occurred during the analysis ($\sigma'_{v,min}$): $r_u = (\sigma'_{v0} - \sigma'_{v,min})/\sigma'_{v0}$. These examples show generally good agreement between r_u and FS_{IB08}. The plots also show how

porewater pressure migration can occur in the model, based on the negative r_u gradient with distance away from the liquefiable layer. The excess porewater pressure migration tends to soften (and in some cases not presented herein, liquefy) otherwise non-liquefiable layers, and further soften the overall site response.

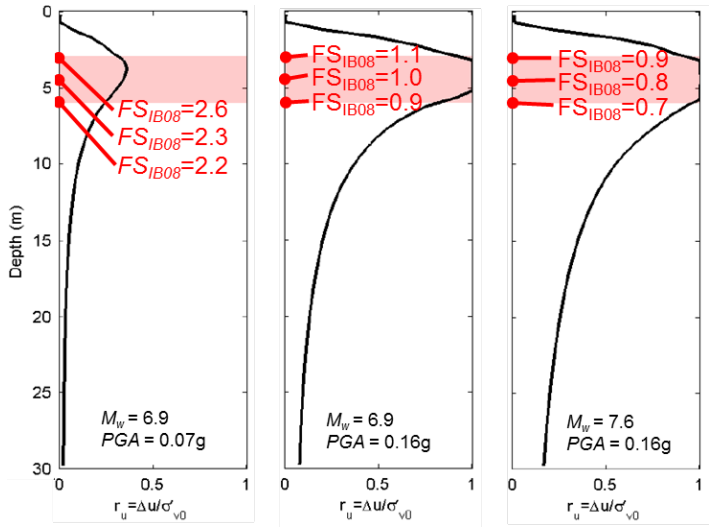

Figure 3. Three examples of maximum excess porewater pressure ratio profiles and calculated factors of safety. The red-shaded zone is the potentially liquefiable layer. All have D_r = 50%, z_{liq} = 3 m, T_{liq} = 3 m, and groundwater is at 1 m.

Figure 4 shows r_u at the middle of the liquefiable layer versus the reciprocal of FS_{IB08}, with the data color-coded by relative density. The gray shaded area in Figure 4 corresponds to Tokimatsu and Seed's (1987) estimates for loose to medium dense soils (Tokimatsu and Yoshimini 1984). The simulation data for D_r of 30% and 50% (e.g., loose to medium dense) follow a similar trend to Tokimatsu and Seed's band, but have more dispersion.

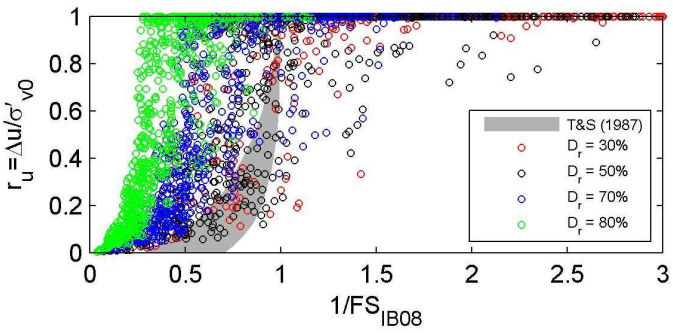

Figure 4. Plots of maximum excess porewater pressure ratio versus liquefaction factor of safety.

For r_u less than 1, the data in Figure 4 show increasing $1/FS_{liq}$ with decreasing relative density. Hence, for sites that do not reach full liquefaction, higher relative densities produce higher r_u values for a given factor of safety. While initially this seems counterintuitive, it is expected based on the element calibration test results as exemplified in Figure 5. The more dilatant

$D_r = 70\%$ sample experiences several cycles of cyclic mobility with elevated (but less than unity) maximum values of r_u prior to reaching liquefaction (defined as 6% double amplitude shear strain in the DSS simulations). In contrast, the looser $D_r = 30\%$ sample is less dilatant, and thus cyclic mobility does not occur until just before liquefaction is reached. At N/N_{liq} less than about 0.95, which is the same domain as $1/FS_{IB} < 1$, the r_u of the $D_r = 70\%$ test is higher than that of the $D_r = 30\%$ test, and this is consistent with the data in Figure 5.

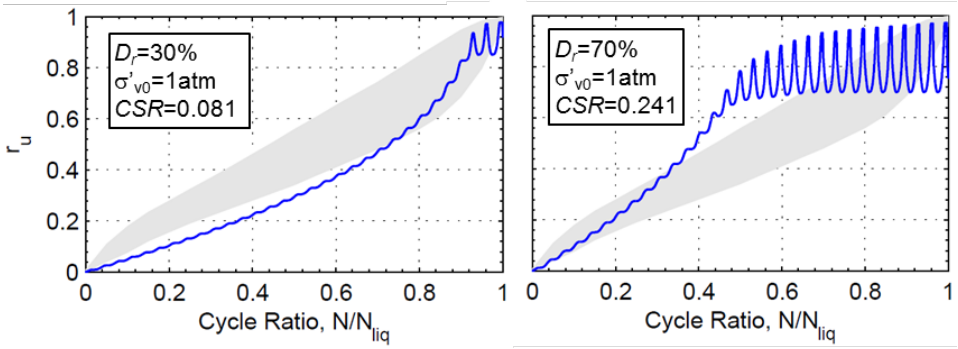

Figure 5. Examples of rates of r_u generation from element calibration CSS simulations.

Figure 4 is useful to examine trends for sites that do not liquefy fully, but the large amount of data clustered at r_u = 1 require a different mode of examination. Figure 6 presents a liquefaction factor of safety cumulative probability density function (CDF) for cases with r_u = 1. The plot is made for a dataset that includes the top, middle and bottom points of the liquefiable layer. This figure shows that about 80 percent of the runs with r_u = 1 had liquefaction $FS_{IB08} \leq 1$.

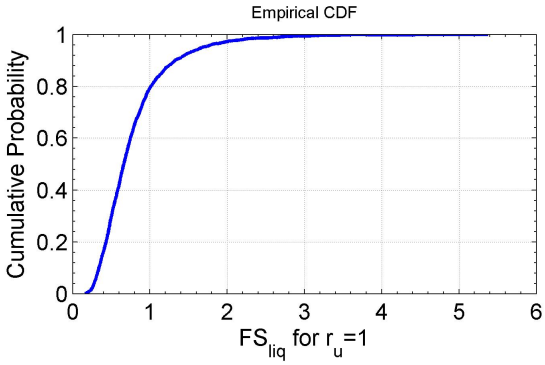

Figure 6. CDF of Idriss & Boulanger (2008) liquefaction factor of safety for cases with r_u = 1.

Conclusions

The site response results show that porewater pressure ratio data for cases that did not reach liquefaction appear to be reasonable and generally follow empirical trends of Tokimatsu and Seed (1987). The Idriss & Boulanger (2008) factor of safety was less than unity for 80 percent of the cases where r_u = 1 occurred in the response model. Based on these results, the element-level calibration essentially held true with respect to liquefaction triggering predictions when employed in the more complex prototype-level site response model. Additional subsurface

profile complexities should be investigated further to discern if the findings from this study are applicable for more general cases.

Acknowledgments

The first author acknowledges and thanks the support provided by Kleinfelder for this research. Partial support was provided by the National Science Foundation CMMI Grant No. 1201195.

References

Abrahamson, N.A., Atkinson, G., Boore, D., Bozorgina, Y., Campbell, K., Chiou, B., Idriss, I., Silva, W. and Youngs, R. (2008). "Comparison of the NGA ground motion relationships," *Eq. Spectra*, **24**(1), pp 45-66.

Ambraseys, N. N. (1988). ''Engineering seismology.'' *Earthquake Engrg. and Struct. Dynamics*, **17**, pp 1–105.

Baker, J.W. (2007). "Quantitative classification of near-fault ground motions using wavelet analysis," *Bulletin of the Seismological Society of America*, **97**(5), pp. 1486-1501.

Brandenberg, S.J., Bellana, N. and Shantz, T. (2010). "Shear wave velocity as function of standard penetration test resistance and vertical effective stress at California bridge sites", *Soil Dyn.and Eq. Engr.*, **30**(2010), pp 1026-1035.

Carlton, B. (2014). "*An Improved Description of the Seismic Response of Sites with High Plasticity Soils, Organic Clays, and Deep Soft Soil Deposits*." PhD dissertation, University of California, Berkeley.

Darendeli, M. (2001). "*A New Family of Normalized Modulus Reduction and Material Damping Curves for Equivalent Linear Analysis*," PhD Dissertation, University of Texas, Austin.

Gingery, J. R., and Elgamal, A. (2013). "Shear Stress-Strain Curves Based on the G/G_{max} Logic: A Procedure for Strength Compatibility," In IACGE 2013, ASCE, *Challenges and Recent Advances in Geotechnical and Seismic Research and Practice*, pp. 721-729.

Gingery, J.R. (2014), "*Effects of Liquefaction on Earthquake Ground Motions*," PhD dissertation draft, University of California, San Diego.

Hardin, B. O. and Drnevich, V. P. (1972). Shear modulus and damping in soils: design equation and curves. *J. Soil Mech. Found. Engng. Div., ASCE* **98**, No. 7, pp 667–691.

Idriss, I.M. and Boulanger, R.W. (2008). *Soil Liquefaction During Earthquakes*, EERI Monograph MNO-12.

Mazzoni, S., McKenna, F., Fenves, G.L. (2010). OpenSees Online Documentation, http://opensees.berkeley.edu/wiki/index.php/Main_Page, Pacific Earthquake Engineering (PEER) Center.

Elgamal, A., Yang, Z. and Parra, E. (2002). "Computational modeling of cyclic mobility and post-liquefaction site response," *Soil Dynamics and Earthquake Engineering*, **22**, pp. 259-271.

Elgamal, A., Yang, Z., Parra, E. and Ragheb, A. (2003). "Modeling of Cyclic Mobility in Saturated Cohesionless Soils," *Int. J. Plasticity*, **19**(6), pp 883-905.

Lysmer, J. and Kuhlemeyer, R.L. (1969). "Finite Difference Model for Infinite Media," *J. Eng. Mech.*, **95** (EMR), pp 859-877.

Power, J. P. (1992). *Construction Dewatering, New methods and Applications*, 2nd Edition, John Wiley & Sons, Inc., New York.

Seyhan, E., Stewart, J.P., Ancheta, T.D., Darragh, R.B. and Graves, R.W. (2014). "NGA-West 2 Site Database," in press *Eq. Spectra*, EERI.

Tokimatsu, K and Seed, H.B. (1987). "Evaluation of settlements in sands due to earthquake shaking," *J. Geotech. Engr.*, **113**(8), pp 861-878.

Tokimatsu, Y. and Yoshimini, K. (1985). "Criteria of soil liquefaction with SPT and fines content," *Proc., 8th World Conf. of Earthq. Engr.*, San Francisco, California, pp 255-262.

Wu, J. (2002). "*Liquefaction triggering and post-liquefaction deformation of Monterey 0/30 sand under uni-directional cyclic simple shear loading*," PhD Dissertation, U.C. Berkeley.

Yang, Z., Elgamal, A., Parra, E. (2003). "Computational model for cyclic mobility and associated shear deformation," *J. of Geotech. and Geoenvr. Engr*., **129** (2), pp 1119-1127.

Yang, Z., Lu, J., Elgamal, A. (2008). *OpenSees Soil Models and Solid-Fluid Coupled Elements*, User's Manual, Version 1.0, UCSD Dept. of Structural Engr.